**SUPPORTING INFORMATION**

# Efficient near-infrared emission benefits from slowing down the internal conversion process

Mingliang Xie,[a] Yannan Zhou, [a] Huayi Zhou, [a] Chengling Ma, [a] Qikun Sun, [a] Shi-Tong Zhang, [c] Yujian Zhang* [b], Wenjun Yang, [a] Shanfeng Xue* [a]

M. Xie, Y. Zhou, H. Zhou, C. Ma, Q. Sun, Prof. S. Xue, Prof. W. Yang

[a]Key Laboratory of Rubber-Plastics of the Ministry of Education, School of Polymer Science & Engineering, Qingdao University of Science and Technology, Qingdao 266042, P. R. China.

E-mail: sfxue@qust.edu.cn

Prof. Y. Zhang

[b]Key Laboratory of the Ministry of Education for Advanced Catalysis Materials, Department of Chemistry, Zhejiang Normal University, Yingbin Road No.688, Jinhua 321004, P. R. China

E-mail: sciencezyj@foxmail.com

Prof. S-T. Zhang

[c]State Key Laboratory of Supramolecular Structure and Materials, Institute of Theoretical Chemistry, College of Chemistry, Jilin University, Changchun 130012, P. R. China.

## Contents

## SI-1 EXPERIMENTAL PROCEDURES

### 1. SYNTHESIS OF TARGET PRODUCTS

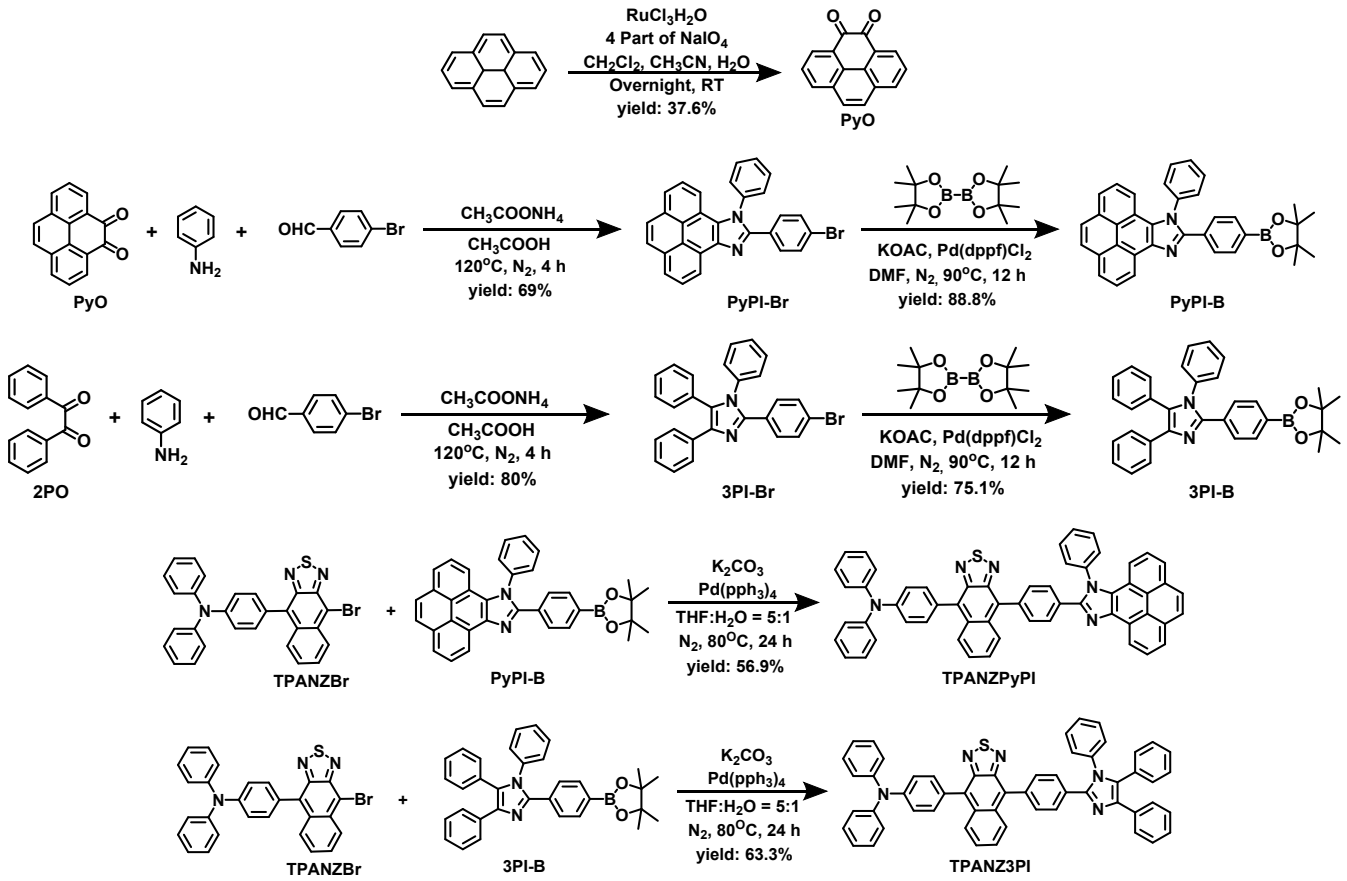


**Scheme S1. Synthesis route of TPANZPyPI and TPANZ3PI.**

Synthesis of pyrene-4,5-dione (PyO): Dissolve the elemental pyrene (2.00 g, 9.89 mmol) in a mixed organic solvent of 40 mL dichloromethane and 40 mL acetonitrile, then add a solution of sodium periodate (9.6 g, 44.88 mmol) dissolved in 50 mL deionized water to the organic phase, and finally add $RuCl_3 \bullet xH_2O$ (0.25 g, 1.21 mmol). The reaction system was stirred overnight at room temperature. After the reaction, the reactants are extracted with a large amount of dichloromethane and saturated salt water. The organic phase is dried with anhydrous magnesium sulfate and filtered. The filtrate is then concentrated through a rotary evaporator and separated by silica gel column chromatography. The drenching agent is dichloromethane: ethyl acetate (60:1; v/v). The product was an orange-red powder (1.1 g) yielding 47.4%. $^1$H NMR (500 MHz, $CDCl_3$) δ 8.39 (d, J = 7.4 Hz, 2H), 8.10 (d, J = 7.9 Hz, 2H), 7.76 (s, 2H), 7.69 (t, J = 7.6 Hz, 2H).

Synthesis of 10-(4-bromophenyl)-9-phenyl-9*H*-pyreno[4,5-d]imidazole (PyPI-Br): A mixture of PyO (1.8 g, 7.68 mmol), aniline (2.80 ml), 4-bromobenzaldehyde (1.42 g, 7.68 mmol) and ammonium acetate (2.96 g, 38.42 mmol) as well as acetic acid (50 ml) was reacted for 4 hours at reflux under nitrogen. At the end of the reaction, filtration was carried out using deionized water as a solvent to obtain a filtrate and dried. It was later purified by silica gel column chromatography using dichloromethane/petroleum ether (5:1; v/v) to give a white powder product (2.51 g) in the 69.04% yield. ($^1$H NMR (500 MHz, $CDCl_3$) δ 9.12 (d, J = 7.5 Hz, 1H), 8.24 (d, J = 7.5 Hz, 1H), 8.20 – 8.10 (m, 2H), 8.07 (t, J = 7.2 Hz, 2H), 7.75 – 7.65 (m, 4H), 7.62 (d, J = 7.3 Hz, 2H), 7.56 (d, J = 8.4 Hz, 2H), 7.49 (d, J = 8.5 Hz, 2H), 7.42 (d, J = 7.9 Hz, 1H).

Synthesis of 9-phenyl-10-(4-(4,4,5,5-tetramethyl-1,3,2-dioxaborolan-2-yl)phenyl)-9*H*-pyreno[4,5-d]imidazole (PyPI-B): A mixture of PyPI-Br (2.50 g, 5.28 mmol), bis(pinacolato)diboron (1.60 g, 6.30 mmol) and potassium acetate (1.54 g g, 15.75 mmol) and the catalyst [1,1 '-bis(diphenylphosphino) ferrocene]dichloropalladium(II) (0.115 g, 0.158 mmol) and a mixture of 1,4-dioxane (50 mL) were reacted under nitrogen at 90 ℃ reflux for 12 hours. At the end of the reaction, it was extracted with dichloromethane and saturated saline, then dried with anhydrous $MgSO_4$ and filtered. It was subsequently purified by silica gel column chromatography using dichloromethane/petroleum

ether (100:1; v/v) to give a white powder product (2.45 g) in 88.83% yield. $^1$H NMR (500 MHz, $CDCl_3$) δ 9.16 (d, J = 7.4 Hz, 1H), 8.23 (d, J = 7.4 Hz, 1H), 8.20 – 8.11 (m, 2H), 8.07 (dd, J = 8.0, 3.9 Hz, 2H), 7.78 (d, J = 8.0 Hz, 2H), 7.72 – 7.60 (m, 8H), 7.43 (d, J = 7.9 Hz, 1H), 1.38 (s, 12H).

Synthesis of 2-(4-bromophenyl)-1,4,5-triphenyl-1*H*-imidazole (3PI-Br): A mixture of 2PO (2.0 g, 9.51 mmol), aniline (3.47 ml), 4-bromobenzaldehyde (1.76 g, 9.51 mmol), and ammonium acetate (3.66 g, 47.55 mmol) as well as acetic acid (80 ml) was reacted for 4 hours at reflux under nitrogen. At the end of the reaction, filtration was carried out using deionized water as a solvent to obtain a filtrate and dried. It was later purified by silica gel column chromatography using dichloromethane/petroleum ether (6:1; v/v) to give a white powder product (3.44 g) in 80% yield. ($^1$H NMR (500 MHz, $CDCl_3$) δ 7.58 (dd, J = 5.2, 3.3 Hz, 2H), 7.39 – 7.35 (m, 2H), 7.31 – 7.26 (m, 5H), 7.26 – 7.17 (m, 6H), 7.12 (dt, J = 3.6, 2.1 Hz, 2H), 7.05 – 7.02 (m, 2H).

Synthesis of 1,4,5-triphenyl-2-(4-(4,4,5,5-tetramethyl-1,3,2-dioxaborolan-2-yl)phenyl)-1*H*-imidazole (3PI-B): A mixture of 3PI-Br (3.12 g, 6.91 mmol), bis(pinacolato)diboron (2.10 g, 8.29 mmol), and potassium acetate (2.04 g g, 20.74 mmol) and the catalyst [1,1 '-bis(diphenylphosphino) ferrocene]dichloropalladium(II) (0.152 g, 0.21 mmol) and a mixture of 1,4-dioxane (70 mL) were reacted under nitrogen at 90 ℃ reflux for 12 hours. At the end of the reaction, it was extracted with dichloromethane and saturated saline, then dried with anhydrous $MgSO_4$ and filtered. It was subsequently purified by silica gel column chromatography using dichloromethane/ ethyl acetate (20:1; v/v) to give a white powder product (3.40 g) in 75.06% yield. ($^1$H NMR (400 MHz, $CDCl_3$) δ 7.67 (d, J = 8.2 Hz, 2H), 7.61 – 7.57 (m, 2H), 7.43 (d, J = 8.2 Hz, 2H), 7.26 – 7.16 (m, 9H), 7.12 (dd, J = 7.8, 1.7 Hz, 2H), 7.05 – 7.01 (m, 2H), 1.32 (s, 12H).

Synthesis of 4-(9-bromonaphtho[2,3-c][1,2,5]thiadiazol-4-yl)-N, N-diphenylaniline (TPANZBr): The TPANZBr comes from our previously reported literature.[1]

Synthesis of N, N-diphenyl-4-(9-(4-(9-phenyl-9*H*-pyreno[4,5-d]imidazol-10-yl)phenyl)naphtho[2,3-c][1,2,5]thiadiazol-4-yl)aniline (TPANZPyPI): TPANZBr (0.81 g, 1.59 mmol), PyPI-B (1.00 g g, 1.91 mmol), potassium carbonate (0.33 g, 2.39 mmol) and catalysts tetrakis(triphenylphosphine)palladium (0.074 g, 0.064 mmol) and a mixture of THF: $H_2O$ (5:1; v/v) were reacted under nitrogen at 80 ℃ for 24 hours. At the end of the reaction, it was extracted with dichloromethane and saturated saline, then dried with anhydrous $MgSO_4$ and filtered. Afterward, it was purified by silica gel column chromatography using dichloromethane/petroleum ether (5:1; v/v) to give a dark red powder product (0.74 g) in the 56.9% yield. $^1$H NMR (500 MHz, $CDCl_3$) δ 9.21 (d, J = 7.4 Hz, 1H), 8.26 (d, J = 7.3 Hz, 1H), 8.23 – 8.14 (m, 3H), 8.09 (dd, J = 8.1, 4.7 Hz, 2H), 8.04 – 7.97 (m, 3H), 7.78 (dd, J = 8.4, 4.9 Hz, 5H), 7.70 (dd, J = 15.3, 7.9 Hz, 3H), 7.58 (d, J = 8.4 Hz, 2H), 7.47 – 7.29 (m, 13H), 7.13 (t, J = 7.2 Hz, 2H). HRMS (ESI) *m/z*: $[M + H]^+$ calcd for $C_{57}H_{35}N_5S$, 822.2691; found, 822.2615.

Synthesis of N,N-diphenyl-4-(9-(4-(1,4,5-triphenyl-1*H*-imidazol-2-yl)phenyl)naphtho[2,3-c][1,2,5]thiadiazol-4-yl)aniline (TPANZ3PI): TPANZBr (0.40 g, 0.79 mmol), 3PI-B (0.47 g, 0.94 mmol), potassium carbonate (0.16 g, 1.18 mmol) and catalysts tetrakis(triphenylphosphine)palladium (0.04 g, 0.031 mmol) and a mixture of THF: $H_2O$ (5:1; v/v) were reacted under nitrogen at 80 ℃ for 24 hours. At the end of the reaction, it was extracted with dichloromethane and saturated saline, then dried with anhydrous $MgSO_4$ and filtered. Afterward, it was purified by silica gel column chromatography using dichloromethane/petroleum ether (5:1; v/v) to give a dark red powder product (0.40 g) in the 63.29% yield. ($^1$H NMR (500 MHz, DMSO) δ 8.05 (d, J = 7.8 Hz, 1H), 7.86 (d, J = 7.8 Hz, 1H), 7.66 (d, J = 8.4 Hz, 2H), 7.60 – 7.54 (m, 6H), 7.49 (t, J = 7.9 Hz, 2H), 7.44 – 7.38 (m, 9H), 7.34 – 7.27 (m, 7H), 7.19 (t, J = 8.2 Hz, 7H), 7.13 (t, J = 7.3 Hz, 2H). $^{13}$C NMR (126 MHz, $CDCl_3$) δ 151.45 (s), 151.28 (s), 147.83 (s), 147.54 (s), 146.45 (s), 138.54 (s), 137.26 (s), 136.47 (s), 134.49 (s), 132.31 – 131.84 (m), 131.24 (d, J = 10.5 Hz), 130.68 (s), 130.36 (s), 129.61 (s), 129.53 – 129.09 (m), 128.75 – 128.30 (m), 128.21 (s), 128.03 (s), 127.34 (d, J = 14.3 Hz), 126.98 (s), 126.67 (s), 126.44 (s), 126.18 (s), 125.18 (s), 123.46 (s), 122.18 (s), 77.29 (s), 77.03 (s), 76.78 (s). HRMS (ESI) *m/z*: $[M + H]^+$ calcd for $C_{55}H_{37}N_5S$, 800.2848; found, 800.2842).

## SI-2 GENERAL METHODS

### 1. GENERAL MEASUREMENTS

The $^1$H NMR spectrum was recorded on a Bruker AC500 spectrometer at 500 and 400 MHz, respectively, using deuterated chloroform ($CDCl_3$) or DMSO as solvents. The chemical shift for each signal was reported in ppm units with tetramethylsilane (TMS) as a standard internal reference. The MALDI-TOF-MS mass spectra were recorded using an AXIMA-CFRTM instrument. UV-vis absorption and fluorescence spectra of solution and film were recorded by a Hitachi U-4100 spectrophotometer and a Hitachi F-4600 spectrophotometer, respectively. An FLS980 spectrometer measured photoluminescence quantum yield. The lifetime was measured on an Edinburgh FLS-1000 spectrometer with an EPL-510 optical laser.

### 2. ELECTROCHEMICAL MEASUREMENTS

Cyclic voltammetry was performed with a BAS 100 W Bioanalytical system, using a glass carbon disk (Φ=3 mm) as the working electrode, a platinum wire as the auxiliary electrode with a porous ceramic wick, and Ag/Ag+ as the reference electrode, standardized for the redox couple ferricinium/ferrocene. All solutions were purged with a nitrogen stream for 10 min before measurement. The procedure was performed at room temperature, and a nitrogen atmosphere was maintained over the solution during the measurements. The energy levels of HOMO and LUMO are calculated according to the Formula below:

$$HOMO = -(E_{ox} \text{ vs. } Ag/Ag^+ - E_{1/2}{}^+ \text{vs.} Ag/Ag^+ + 4.8)\ eV$$

$$LUMO = -(E_{red} \text{ vs. } Ag/Ag^+ - E_{1/2}{}^- \text{vs.} Ag/Ag^+ + 4.8)\ eV$$

the $E_{ox}$ vs. $Ag/Ag^+$ and $E_{red}$ vs. $Ag/Ag^+$ are oxidation and reduction onset potentials relative to the $Ag/Ag^+$ electrode, respectively. Ferrocene was used as an internal standard. $E_{1/2}{}^+$ vs. $Ag/Ag^+$ and $E_{1/2}{}^-$ vs. $Ag/Ag^+$ are half-wave potentials of $Fc^+/Fc$ obtained from positive and negative CV scans, respectively. The $E_{1/2}{}^+$ vs.$Ag/Ag^+$ is 0.21 V, and $E_{1/2}{}^-$ vs.$Ag/Ag^+$ is 0.08 V.

### 3. THERMAL STABILITY MEASUREMENTS

Thermal gravimetric analysis (TGA) of the material was performed using a Perkin-Elmer thermal analysis system from 30 to 650 ℃ at a heating rate of 10 ℃/min under the nitrogen atmosphere. The Differential Scanning Calorimeter (DSC) test uses DSC204F1 produced by a German thermal analysis instrument company, which rises to the melting point at a heating rate of 10 ℃/min starting from 25 ℃ under nitrogen flow, then cools down to 25 ℃ at a rate of 20 ℃/min, and then undergoes secondary heating. The first heating is to obtain the product's melting point and eliminate the heat history. During the second heating, the product becomes amorphous in order to observe whether there is a glass transition temperature in the product.

### 4. THEORETICAL CALCULATION

The geometric configuration optimization and electron density distribution of the ground state and excited state of emitters were obtained using the PBE0/6-31G (d, p) method based on Gaussian density functional theory (DFT) and time-dependent density functional theory (TD-DFT). The rate of the RISC process between $T_n$ and $S_1$ states can be calculated using the semiclassical Marcus theory and Fermi's golden rule.[2-6] The internal conversion rate is calculated using fcclasses software, where the vibronic nonadiabatic coupling (NAC) matrix elements between the $T_1$ and $T_2$ states can be calculated by the Hellmann–Feynman coupling[7] in the ESD module of the ORCA 5.03 package.[8] The reverse intersystem crossing rate is calculated based on the assumption in the literature that the recombination energy between two excited state structures is 0.1 eV.[9]

### 5. DEVICE FABRICATION AND CHARACTERIZATION

Before the measurement, vacuum sublimation obtained the target molecules as pure products. TPBi used in the device was purchased from Jilin OLED Material Tech Co., Ltd., and HATCN, TAPC, TCTA, and MADN were purchased from Xi'an Polymer Light Technology Corp. PPI33PBO comes from our previous report.[10] ITO-coated glass with a sheet resistance of 10 Ω square$^{-1}$ was used as the substrate. The pre-treatment of ITO glass included a routine chemical cleaning using detergent and alcohol in sequence, dried in an oven at 120 ℃. After the oxygen plasma was cleaned for 7 min and finally transferred to a vacuum deposition system with a base pressure greater than 1.6 ×

$10^{-4}$ Pa for organic and metal deposition. The current–voltage–brightness characteristics were measured by using a Keithley source measurement unit (Keithley 2450 and LS-160) The electroluminescent (EL) spectra and Commission Internationale de l'Eclairage (CIE) coordinates of these devices were measured with a Flame-S (Serial Number: FLMS16791). EQEs were calculated from the luminance, current density, and EL spectrum.

## SI-3 SUPPLEMENTARY FIGURES

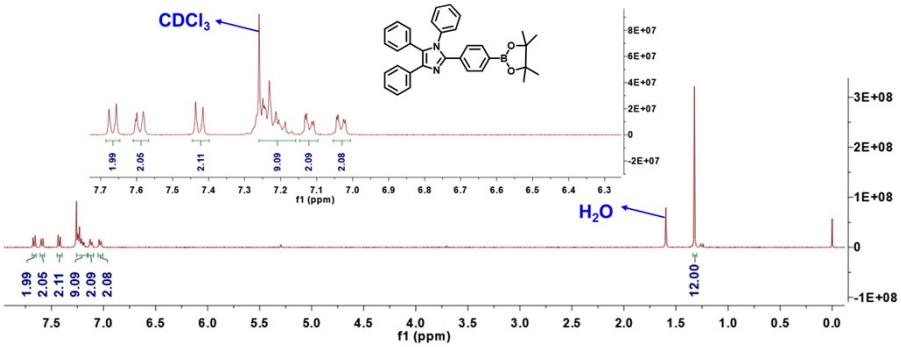


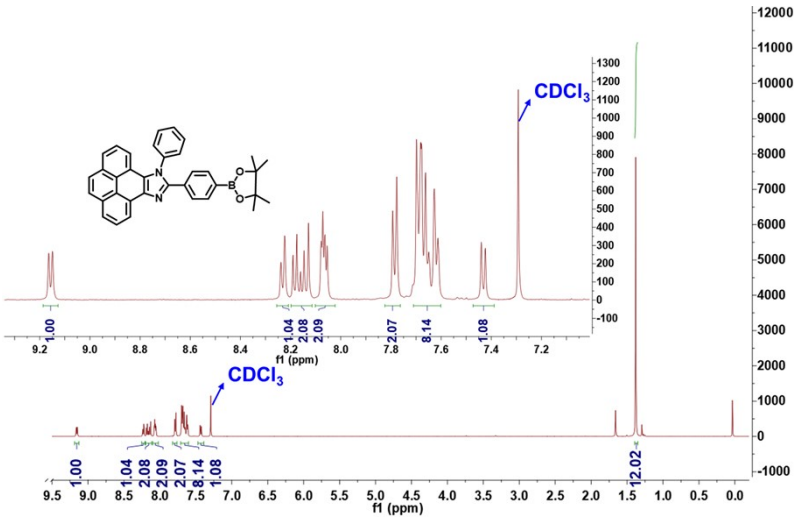


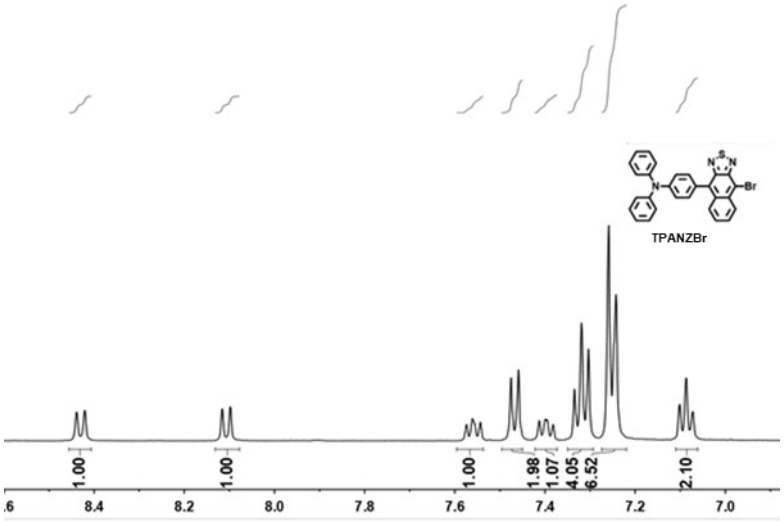

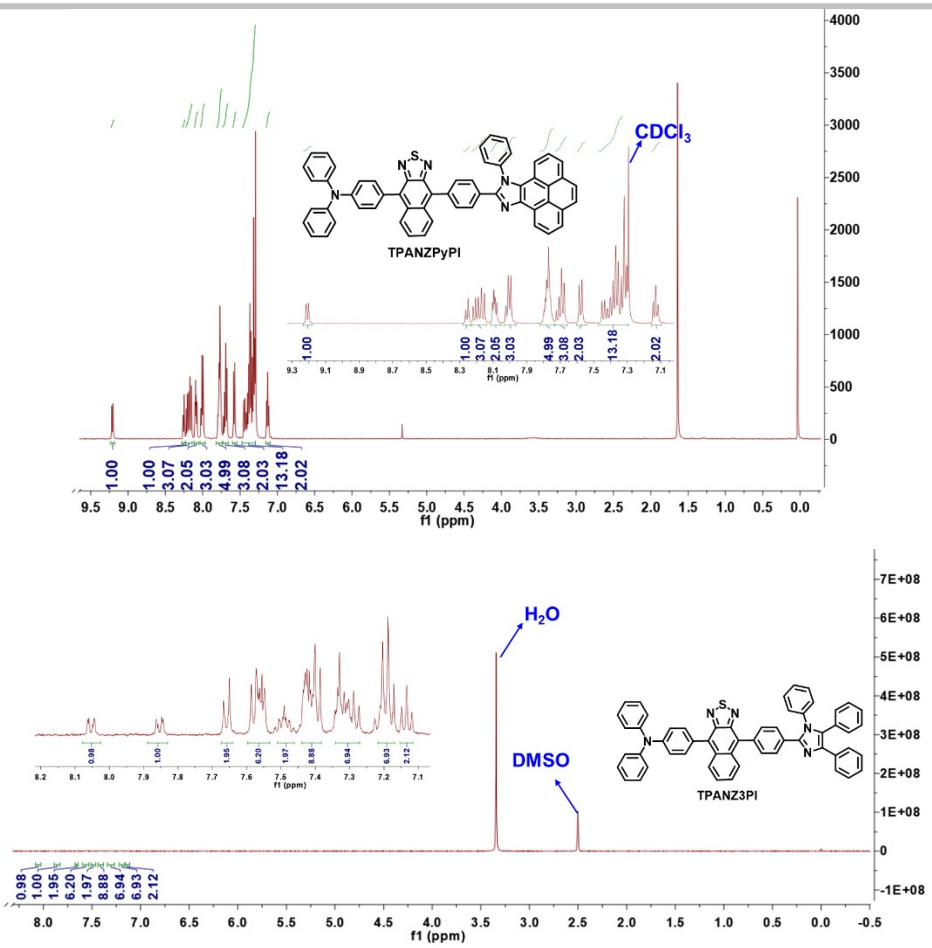


**Figure S1. $^{1}$H-NMR Spectrum of intermediate products, TPANZPyPI in $CDCl_3$ and TPANZ3PI in DMSO.**

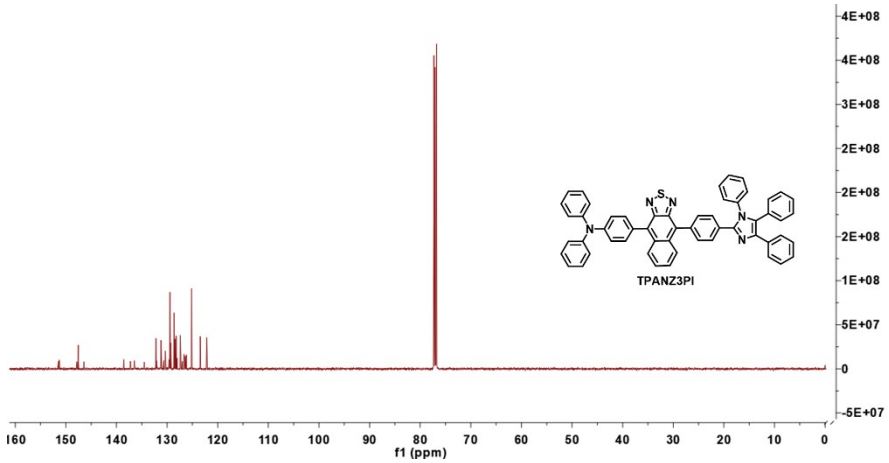


**Figure S2. $^{13}$C-NMR Spectrum of TPANZ3PI in $CDCl_3$.**

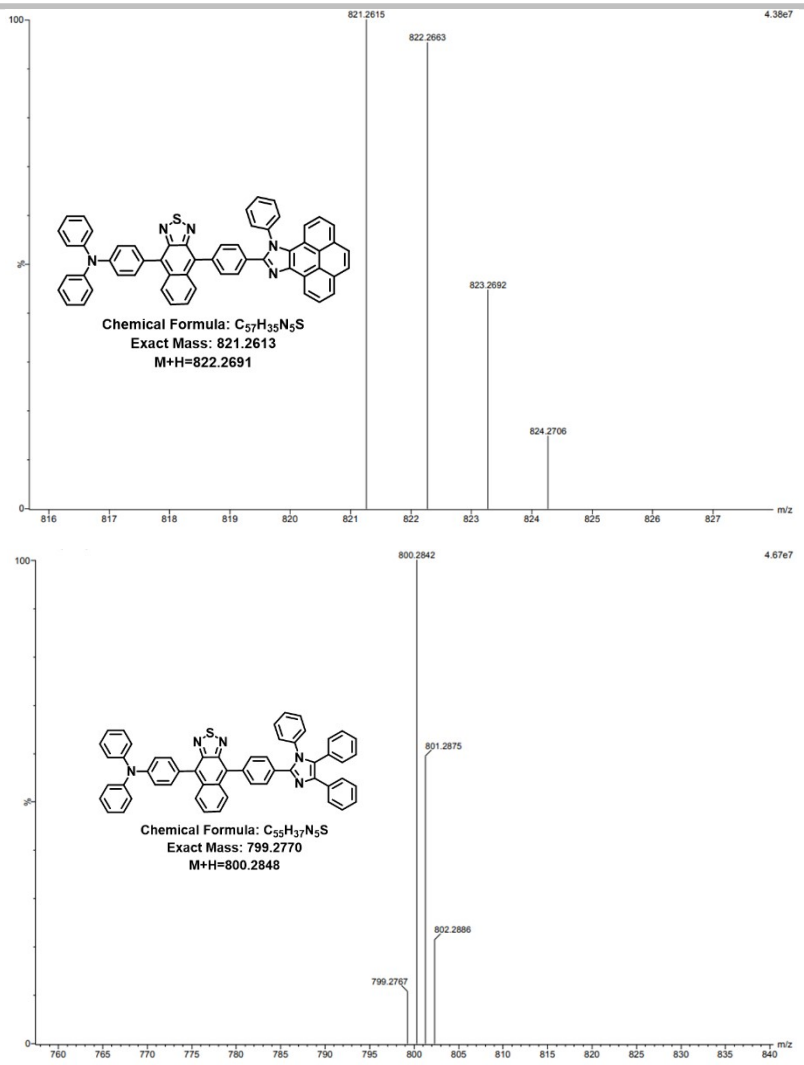


**Figure S3. Mass Spectrum $(M+H)^+$ of TPANZPyPI and TPANZ3PI.**

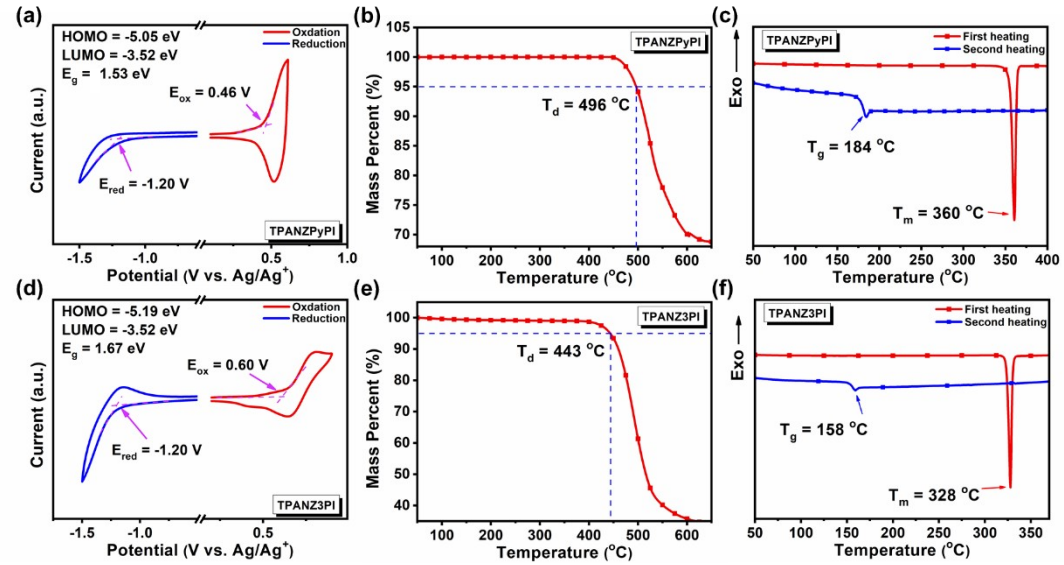


**Figure S4. The cyclic voltammetry (CV) curves and the thermogravimetric analysis (TGA) curve and the differential scanning calorimeter (DSC) of the TPANZPyPI and TPANZ3PI.**

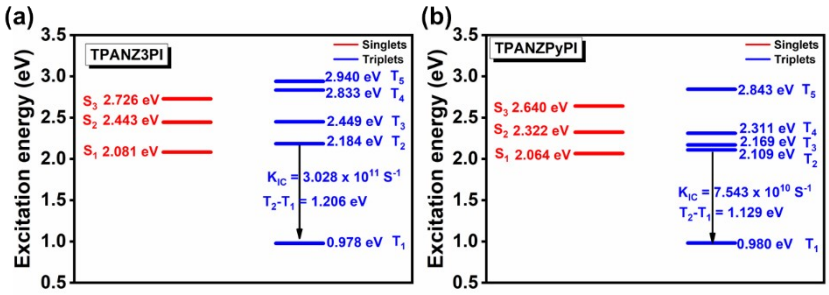


**Figure S5. The energy level diagram of (a) TPANZ3PI and (b) TPANZPyPI.**

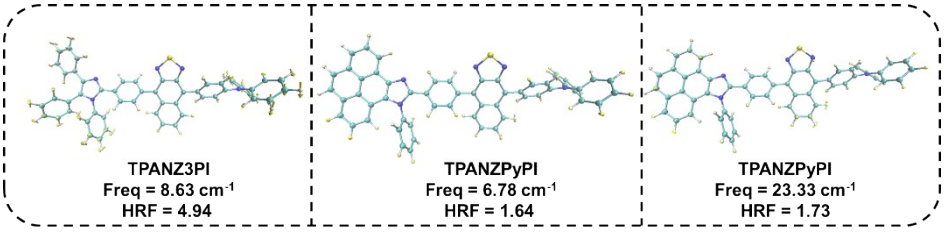


**Figure S6. The representative vibration modes for $S_1 \rightarrow S_0$ transition of TPANZ3PI and TPANZPyPI.**

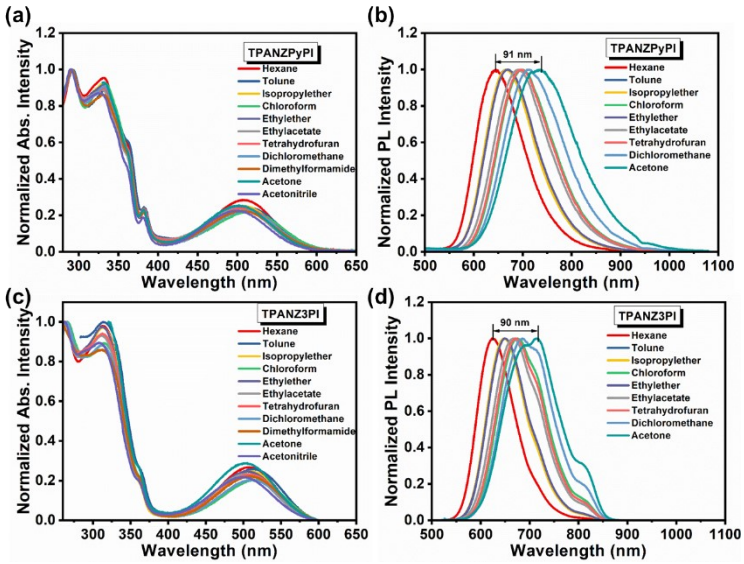


**Figure S7. The (a) UV-Vis and (b) PL spectra of TPANZPyPI in different solutions.**

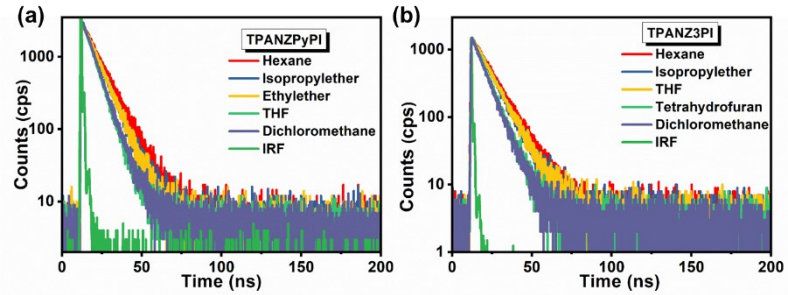


**Figure S8. The transient PL decay spectra of TPANZPyPI and TPANZ3PI in different solvents.**

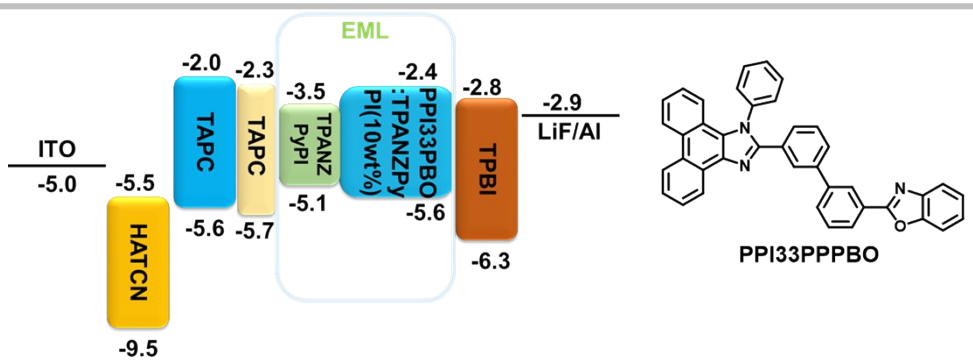


**Figure S9. Devices architecture, energy diagram, and functional layers for the vacuum-deposited OLEDs.**

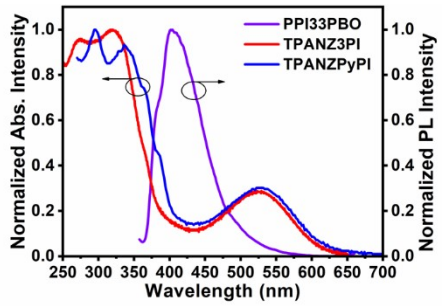


**Figure S10. Emission spectra of PPI33PBO film and absorption spectra of TPANZPyPI and TPANZ3PI film.**

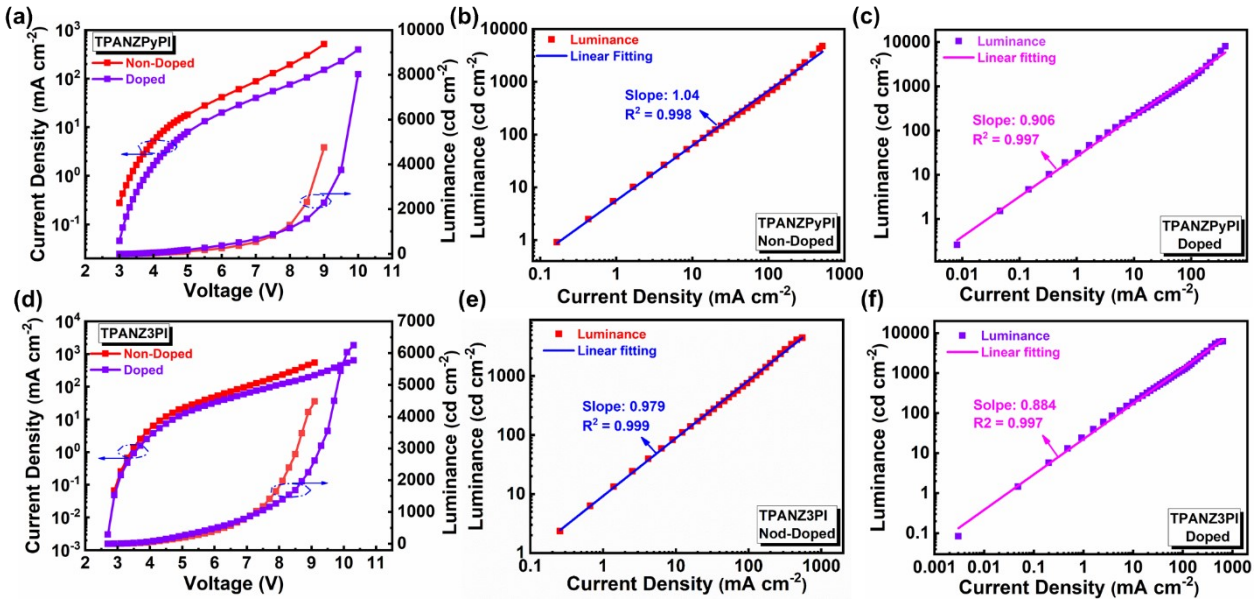


**Figure S11. (a) and (d) Current density-voltage-luminance curves of non-doped and doped devices; (b) and (e) Current density-luminance curve of non-doped device; (c) and (f) Current density-luminance curve of the doped device.**

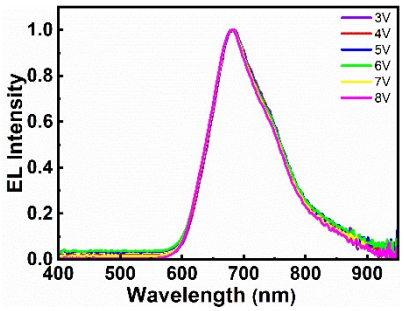

**Figure S12. Electroluminescence spectra of TPANZPyPI non-devices at different voltages.**

## SI-4 SUPPLEMENTARY TABLES

**Table S1. The TPANZPyPI and TPANZ3PI top ten singlet excited state energies.**

| Excitation [eV] | $S_1$ | $S_2$ | $S_3$ | $S_4$ | $S_5$ | $S_6$ | $S_7$ | $S_8$ | $S_9$ | $S_{10}$ |
|---|---|---|---|---|---|---|---|---|---|---|
| TPANZPyPI | 2.064 | 2.322 | 2.640 | 3.301 | 3.455 | 3.497 | 3.626 | 3.666 | 3.751 | 3.795 |
| TPANZ3PI | 2.081 | 2.443 | 2.726 | 3.642 | 3.667 | 3.725 | 3.791 | 3.880 | 3.898 | 3.953 |

**Table S2. The TPANZPyPI and TPANZ3PI top ten triplet excited state energies.**

| Excitation [eV] | $T_1$ | $T_2$ | $T_3$ | $T_4$ | $T_5$ | $T_6$ | $T_7$ | $T_8$ | $T_9$ | $T_{10}$ |
|---|---|---|---|---|---|---|---|---|---|---|
| TPANZPyPI | 0.980 | 2.109 | 2.169 | 2.311 | 2.843 | 2.948 | 3.008 | 3.055 | 3.118 | 3.213 |
| TPANZ3PI | 0.978 | 2.184 | 2.449 | 2.833 | 2.940 | 3.009 | 3.052 | 3.116 | 3.140 | 3.442 |

**Table S3. The photoluminescence quantum yield ($\Phi_F$) and emission peak of TPANZPyPI and TPANZ3PI in different solvents.**

| | $\lambda_{PL,TPANZPyPI}$ [nm] | $\lambda_{PL,TPANZ3PI}$ [nm] | $\Phi_{F,\ TPANZPyPI}$ [%] | $\Phi_{F,\ TPANZ3PI}$ [%] |
|---|---|---|---|---|
| Hexane | 645 | 623 | 86.8 | 88.6 |
| Toluene | 665 | 648 | 75.4 | 81.6 |
| Isopropylether | 667 | 648 | 67.2 | 75.2 |
| Chloroform | 700 | 675 | 49.3 | 60.6 |
| Ethylether | 670 | 649 | 63.6 | 72.6 |
| Ethylacetate | 690 | 667 | 46.9 | 54.5 |
| Tetrahydrofuran | 698 | 671 | 43.7 | 51.5 |
| Dichloromethane | 709 | 685 | 40.9 | 42.6 |

**Table S4. Color coordinates of TPANZPyPI non-doped devices at different voltages.**

| Voltage | 3V | 4V | 5V | 6V | 7V | 8V | 9V |
|---|---|---|---|---|---|---|---|
| CIE [x,y] | 0.6963 | 0.6981 | 0.6964 | 0.6981 | 0.6950 | 0.6943 | 0.6928 |
| | 0.2393 | 0.2993 | 0.2999 | 0.3002 | 0.3003 | 0.3013 | 0.3027 |

## SI-5 REFERENCES


[1] Y. Yu, X. Chao, M. Xie, Y. Zhou, C. Ma, H. Zhou, Q. Sun, Y. Pan, W. Yang, S. Xue, *Dyes. Pigm.*, 2023, 215, 111306.

[2] R. A. Marcus, *J. Chem. Phys.*, 1956, 24, 966–978.

[3] R. Marcus and N. Sutin, Biochim. Biophys. Acta, *Rev. Bioe-nerg.*, 1985, 811, 265–322.

[4] V. Lawetz, G. Orlandi and W. Siebrand, *J. Chem. Phys.*, 1972, 56, 4058–4072.a

[5] G. W. Robinson and R. P. Frosch, J. Chem. Phys., 1963, 38, 1187–1203.

[6] J. Li, M. Zhang, T. Li, D. Guo, T. Tian, H. Zhang, J. Mater. Chem. C, 2022, 10, 13124–13136.

[7] Z. Li and W. Liu, J. Chem. Phys., 2014, 141, 014110.

[8] F. Neese, Wiley Interdiscip. Rev.: Comput. Mol. Sci., 2018, 8, e1327.

[9] J. Li, M. Zhang, T. Li, D. Guo, T Tian, H. Zhang, J. Mater. Chem. C, 2022, 10, 13124–13136.

[10] C. Liu, T. Li, M. Sun, M. Xie, Y. Zhou, W. Feng, Q. Sun, S-T. Zhang, S. Xue, W. Yang, *Adv. Funct. Mater.,* 2023, 33, 2215066.